Mon. Not. R. Astron. Soc. **000**, 000–000 (0000) Printed 8 May 2019 (MN LATEX style file v2.2)

Late time-transition redshift as cosmic parameter for the accelerated expansion of the universe

Abraão J. S. Capistrano⋆

Applied physics Master program, Federal University of Latin-American Integration, 85867-670, P.o.b: 2123, Foz do iguassu-PR, Brazil
Casimiro Montenegro Filho Astronomy Center, Itaipu Technological Park, 85867-900, Foz do Iguassu-PR, Brazil

ABSTRACT

Using a joint statistical analysis, we test a five-dimensional embedded model based on the Nash-Greene embedding theorem at late-time transition redshift. Performing a Markov Chain Monte Carlo (MCMC) modelling, we combine observational data sets as those of the recent Pantheon type Ia supernovae, Baryon Acoustic Oscillations (BAO) and the angular acoustic scale of the Cosmic Microwave Background (CMB) to impose restrictions on the model and correlating the model parameters to mimicking an equation of state. From statistical classifiers as the Akaike Information Criterion (AIC) and Bayesian Information Criterion (BIC), we use the Jeffreys' scale and find a strong evidence favoring a statistically consistence a dynamical Dark energy (CPL parameterization) and a relative consistence with the ΛCDM model and wCDM model. Moreover, we find that the transition redshift used as a cosmic discriminator with the best fit $z_t = 1.53 \pm 0.17$ at 1-σ C.L. with a range scenario for sharp late transitions.

Key words: modified Friedman equations, modified gravity, dark energy

1 INTRODUCTION

The true mechanism behind the accelerated phase of the universe remains an open question. After more than 20 years since the very first evidence of the cosmic accelerated expansion, one of the pivotal directions of investigations are about to unravel whether the dark energy equation of state (EoS), with the main fluid parameter $w(z)$, is restricted to the value $w_0 = -1$, as suggested by observations (Planck Collaboration, 2015), in conformity with the very popular ΛCDM model, or there would be any deviations from that value leading to dynamical dark energy models. Even though its success, the ΛCDM model lacks of an underlying physical understanding, since the Cosmological constant Λ and the Cold dark matter (CDM) are problems of their own (Nemiroff, Joishi and Atla, 2015; Santos, Coley, Devi and Alnaniz, 2017; Kumar and Singh, 2017; Velten, vom Marttens and Zimdahl, 2014; Sultana, 2016; Sivanandam, 2013; Nozari, Behrouz and Rashidi, 2014). Hence, an equation of state is plays a fundamental role to confront a model to observational data commonly performed with statistical methods. Interestingly, it has been suggested that the dark energy equation may have a late-time phase transition (Martins and Colomer, 2016, 2018, 2019) with $z \gtrsim 1$. This induces to an interesting scenario departing from the non-dynamical ΛCDM cosmology since at high redshifts the constraints are weaker (Hill, Schramm and Fry, 1988; Bassett, Kunz, Silk and Ungarelli, 2002; Parker and Raval, 1999, 2000; Mortonson, Hu and Huterer, 2009; Di Valentino, Linder and Melchiorri, 2018; Durrive, Ooba, Ichiki and Sugiyama, 2018; Martins and Colomer, 2018).

The theoretical background in this paper concerns the possibility that the universe might be embedded in extra dimensions and dark energy can be explained as a geometric outcome from the extrinsic curvature. Most of these extra dimensional models have been Kaluza-Klein or/and string inspired, such as, for instance, the Arkani-Hamed, Dvali and Dimopolous (ADD) model (Arkani-Hamed, Dimopoulos and Dvali, 1998), the Randall-sundrum model (Randall and Sundrum, 1999a,b) and the Dvali-Gabadadze-Porrati model (DPG) (Dvali, Gabadadze, and Porrati, 2000). Differently form these models and variants, we investigate how the embedding as a prior mathematical structure can be suited for construction of a physical theory, keeping no relation with brane or string proposals. Several authors have been explored this possibility in many contexts (Battye and Carter, 2001; Maia and Monte, 2002; Maia, Monte, Maia and Alcaniz, 2005; Maia, Silva and Fernandes, 2007; Heydari-Fard, Sepangi, 2007; Jalalzadeh, Mehrnia and Sepangi, 2009; Maia, Capistrano, Alcaniz and Monte, 2011; Ranjbar, Sepangi and Shahidi, 2012; Capistrano and Cabral, 2014; Capistrano, 2015; Capistrano, Gutiérrez-Pieres, Ulhoa and Amorim, 2017; Capistrano, 2017; Maia and Monte, 2002; Maia, Monte, Maia and Alcaniz, 2005; Maia, Silva and Fernandes, 2007).

This paper aims at investigating in a late-time tran-

⋆ E-mail:abraao.capistrano@unila.edu.br

 doi:10.20944/preprints201905.0097.v1

sition redshift on how the cosmological parameters, mainly on the current matter density Ω_{m0}, the physical baryon density $100\Omega_b h^2$ and the dimensionless Hubble parameter h, are accommodated in the present proposed model under this assumption and whether the current surveys on dark energy constraint the parameters to favor or not a phase transition over some popular models as the ΛCDM, quintessense (wCDM) (Caldwell, Dave and Steinhardt, 2018; Ratra and Peebles, 1988) and Chevallier-Polarski-Linder (CPL) (Chevallier and Polarski, 2001; Linder, 2003) parameterisations. To analyse the background data, we perform the Markov Chain Monte Carlo (MCMC) sample technique with a modified code from (Luna, Basilakos and Nesseris, 2018; Arjona, Cardona and Nesseris, 2019) using the joint likelihood of kinematical probes as of the Cosmic Microwave Background (CMB) Planck 2015 data (Planck Collaboration, 2015), the largest dataset Pantheon SnIa (Scolnic et al., 2018) with redshift ranging from $0.01 < z < 2.3$ that guarantees a low and intermediate redshift data, the Hubble parameter as a function of redshift ($H(z)$)(Zhang et al., 2014; Stern et al., 2010; Moresco et al., 2012; Chuang and Wang, 2013; Moresco, 2015; Delubac et al., 2015) and Baryonic Acoustic Oscillations (BAO) from points of the joint surveys 6dFGS (Beutler et al., 2011), SDDS (Anderson et al., 2014), BOSS CMASS (Xu et al. 2012), WiggleZ (Blake et al., 2012), MSG (Ross et al., 2015) and BOSS DR12 (Gil-Marín et al., 2016).

The paper is organized as follows: in the second section, we make a brief review on the theoretical framework. The third section presents the cosmological analysis and outcomes by using the Akaike Information Criterion (Akaike, 1974) and Bayesian criteria (Schwarz, 1978) on the resulting contours confidence regions. In the final section, we conclude with our final remarks and prospects.

2 THE THEORETICAL FRAMEWORK

The gravitational action functional in the presence of confined matter field on a four-dimensional embedded space with thickness l embedded in a D-dimensional ambient space (bulk) has the form

$$S = -\frac{1}{2\kappa_D^2}\int \sqrt{|\mathcal{G}|}\mathcal{R}d^D x - \int \sqrt{|\mathcal{G}|}\mathcal{L}_m^* d^D x \,, \tag{1}$$

where κ_D^2 is the fundamental energy scale on the embedded space, $\mathcal{R}$ denotes de Ricci scalar of the bulk and $\mathcal{L}_m^*$ is the confined matter lagrangian. In this model, the matter energy momentum tensor occupies a finite hypervolume with constant radius l along the extra-dimensions. The variation of Einstein-Hilbert action in Eq.(1) with respect to the bulk metric $\mathcal{G}_{AB}$ leads to the Einstein equations for the bulk

$$\mathcal{R}_{AB} - \frac{1}{2}\mathcal{G}_{AB} = \alpha^\star \mathcal{T}_{AB} \,, \tag{2}$$

where $\alpha^\star$ is energy scale parameter and $\mathcal{T}_{AB}$ is the energy-momentum tensor for the bulk (Maia, Monte, Maia and Alcaniz, 2005; Maia, Silva and Fernandes, 2007; Maia, Capistrano, Alcaniz and Monte, 2011). To generate a thick embedded space-time is important to perturb the related background and it should be done in accordance with the confinement hypothesis of gauge interactions that depends only on the four-dimensionality of the space-time (Donaldson, 1985; Taubes, 1984), even though a mathematical extension of a gauge theory to a higher dimensional space is possible, we adopt the current phenomenology that imposes the fourth dimensionality of space-time (Lim, 2014).

Nash's original embedding theorem (Nash, 1956) used a flat D-dimensional Euclidean space, later generalized to any Riemannian manifold including non-positive signatures by Greene (Greene, 1970) with independent orthogonal perturbations. This choice of perturbations facilitates to get to a differentiable smoothness of the embedding between the manifolds, which is a primary concern of Nash's theorem and satisfies the Einstein-Hilbert principle, where the variation of the Ricci scalar is the minimum as possible. Hence, it guarantees that the embedded geometry remains smooth (differentiable) after smooth (differentiable) perturbations. With all these concepts, let us consider a Riemannian manifold V_4 with a non-perturbed metric $\bar{g}_{\mu\nu}$ being locally and isometrically embedded in a n-dimensional Riemannian manifold V_n given by a differentiable and regular map $\mathcal{X} : V_4 \to V_n$ satisfying the embedding equations

$$\mathcal{X}^A_{,\mu}\mathcal{X}^B_{,\nu}\mathcal{G}_{AB} = \bar{g}_{\mu\nu} \,, \tag{3}$$

$$\mathcal{X}^A_{,\mu}\bar{\eta}^B_a\mathcal{G}_{AB} = 0 \quad , \tag{4}$$

$$\bar{\eta}^A_a\bar{\eta}^B_b\mathcal{G}_{AB} = \bar{g}_{ab} \,. \tag{5}$$

where we have denoted by $\mathcal{G}_{AB}$ the metric components of V_n in arbitrary coordinates, $\bar{\eta}$ denotes a non-perturbed unit vector field orthogonal to V_4. Concerning notation, capital Latin indices run from 1 to n. Small case Latin indices refer to the only one extra dimension considered. All Greek indices refer to the embedded space-time counting from 1 to 4. Those set of equations represent the isometry condition Eq.(3), orthogonality between the embedding coordinates $\mathcal{X}$ and $\bar{\eta}$ in Eq.(4), and also, the vector normalization $\bar{\eta}$ and $\bar{g}_{ab} = \epsilon_a\delta_{ab}$ with $\epsilon_a = \pm 1$ in which the signs represent the signatures of the extra-dimensions. Hence, the integration of the system of equations Eqs.(3), (4) and (5) assures the configuration of the embedding map $\mathcal{X}$.

The second fundamental form, or more commonly, the non-perturbed extrinsic curvature $\bar{k}_{\mu\nu}$ of V_4 is by definition the projection of the variation of $\bar{\eta}$ onto the tangent plane :

$$\bar{k}_{\mu\nu} = -\mathcal{X}^A_{,\mu}\bar{\eta}^B_{,\nu}\mathcal{G}_{AB} = \mathcal{X}^A_{,\mu\nu}\bar{\eta}^B\mathcal{G}_{AB} \,, \tag{6}$$

where the comma denotes the ordinary derivative.

2.1 The background cosmological model

To obtain the embedded four-dimensional equations, one can take Eq.(2) written in the Gaussian frame embedding veilbein $\{\mathcal{X}^A_\mu, \eta^A_a\}$. This reference frame is composed by a regular and differentiable coordinate $\{\mathcal{X}^A_\mu\}$ and a unitary normal vector $\{\eta^A_a\}$. Accordingly, they define the basis of the embedded geometry and one can obtain the embedded four-dimensional field equations

$$R_{\mu\nu} - \frac{1}{2}Rg_{\mu\nu} - Q_{\mu\nu} = -8\pi G T_{\mu\nu} \,, \tag{7}$$

$$k^{\ \rho}_{\mu;\rho} - h_{,\mu} = 0 \,, \tag{8}$$

where the semi-colon denotes a covariant derivative. The $T_{\mu\nu}$ tensor is the four-dimensional energy-momentum tensor of

Preprints (www.preprints.org) | NOT PEER-REVIEWED | Posted: 8 May 2019 doi:10.20944/preprints201905.0097.v1

a perfect fluid, expressed in co-moving coordinates as

$$T_{\mu\nu} = (p+\rho)U_\mu U_\nu + p\, g_{\mu\nu}, \quad U_\mu = \delta^4_\mu \,,$$

where U_μ is the co-moving four-velocity.

Differently what happens to the usual general Relativity framework, a natural embedding between space-times leads to the appearance of the extrinsic terms. The deformation tensor $Q_{\mu\nu}$ is a geometrical term given by

$$Q_{\mu\nu} = g^{\rho\sigma}k_{\mu\rho}k_{\nu\sigma} - k_{\mu\nu}H - \frac{1}{2}\left(K^2 - h^2\right)g_{\mu\nu} \,, \tag{9}$$

where we denote $h = g^{\mu\nu}k_{\mu\nu}$ and $h^2 = h.h$ is the mean curvature. The term $K^2 = k^{\mu\nu}k_{\mu\nu}$ is the Gaussian curvature. It follows that $Q_{\mu\nu}$ is conserved in the sense of Noether's theorem

$$Q^{\mu\nu}{}_{;\nu} = 0 \,. \tag{10}$$

Moreover, we work with a spatially Friedman-Lemaître-Robertson-Walker (FLRW) geometry with line element expressed in coordinates (r,θ,ϕ,t) in such a way

$$ds^2 = -dt^2 + a^2\left[dr^2 + f^2_\kappa(r)\left(d\theta^2 + \sin^2\theta d\varphi^2\right)\right] \,, \tag{11}$$

where $f(r)_\kappa = \sin r$, r,$\sinh r$. Since the FLRW geometry can be locally embedded in five-dimensions, it can be regarded as a four-dimensional hypersurface dynamically evolving in a flat five-dimensional bulk whose Riemann tensor $\mathcal{R}_{ABCD}$ is

$$\mathcal{R}_{ABCD} = 0 \,, \tag{12}$$

where $\mathcal{G}_{AB}$ denotes the bulk metric components in arbitrary coordinates. Hence, with a flat dimensional bulk, concerning our cosmological applications, we are not considering the appearance of the cosmological constant Λ.

Using Eq.(11), one obtains a solution for Eq.(8) that is given by

$$k_{ij} = \frac{b}{a^2}g_{ij}, \quad i,j = 1,2,3, \quad k_{44} = \frac{-1}{\dot{a}}\frac{d}{dt}\frac{b}{a},$$

where the extrinsic bending function $b(t) = k_{11}$ is function of time. The dot symbol denotes an ordinary time derivative. This arbitrariness follows from the confinement of the four-dimensional gauge fields, which produces the homogeneous equation as shown in Eq.(8).

Denoting the usual Hubble parameter by $H = \dot{a}/a$ and the extrinsic parameter $B = \dot{b}/b$, one obtains

$$k_{ij} = \frac{b}{a^2}g_{ij}, \quad k_{44} = -\frac{b}{a^2}(\frac{B}{H} - 1), \tag{13}$$

$$K^2 = \frac{b^2}{a^4}\left(\frac{B^2}{H^2} - 2\frac{B}{H} + 4\right), \quad h = \frac{b}{a^2}(\frac{B}{H} + 2) \tag{14}$$

$$Q_{ij} = \frac{b^2}{a^4}\left(2\frac{B}{H} - 1\right)g_{ij}, \; Q_{44} = -\frac{3b^2}{a^4}, \tag{15}$$

$$Q = -(K^2 - h^2) = \frac{6b^2}{a^4}\frac{B}{H} \,, \tag{16}$$

where in Eq.(15), we have denoted $i,j = 1..3$, with no sum in indices. For simplicity, we denote the expansion parameter as $a(t) = a$ and the bending function as $b(t) = b$.

Since the dynamics equations for the extrinsic curvature are not complete in five-dimensions, motivated by the lack of uniqueness of the function $b(t)$, and being the extrinsic curvature independent rank-2 field, one can derive the Einstein-Gupta equations (Gupta, 1954; Maia, Capistrano, Alcaniz and Monte, 2011) in a form

$$\mathcal{F}_{\mu\nu} = 0 \,, \tag{17}$$

where they are defined as a copy (concerning its structure) of the usual Riemannian geometry. Hence, once can define a "f-Riemann tensor"

$$\mathcal{F}_{\nu\alpha\lambda\mu} = \partial_\alpha\Upsilon_{\mu\lambda\nu} - \partial_\lambda\Upsilon_{\mu\alpha\nu} + \Upsilon_{\alpha\sigma\mu}\Upsilon^\sigma_{\lambda\nu} - \Upsilon_{\lambda\sigma\mu}\Upsilon^\sigma_{\alpha\nu} \,,$$

$$\Upsilon_{\mu\nu\sigma} = \frac{1}{2}\left(\partial_\mu f_{\sigma\nu} + \partial_\nu f_{\sigma\mu} - \partial_\sigma f_{\mu\nu}\right) \,,$$

$$\Upsilon_{\mu\nu}{}^\lambda = f^{\lambda\sigma}\Upsilon_{\mu\nu\sigma}.$$

that were constructed from a "connection" associated with $k_{\mu\nu}$ and

$$f_{\mu\nu} = \frac{2}{K}k_{\mu\nu}, \quad \text{and} \quad f^{\mu\nu} = \frac{2}{K}k^{\mu\nu} \,, \tag{18}$$

in such a way that the normalization condition $f^{\mu\rho}f_{\rho\nu} = \delta^\mu_\nu$ applies.

2.2 The modified Friedman equation

Taking Eq.(11) in Eq.(17), ones obtains the contribution $\frac{B}{H} = 1 \pm \sqrt{|4\eta_0 a^4 - 3|}$, and with the results from Eqs.(7), (8) and (10), the Friedman equation modified by the extrinsic curvature can be written as

$$\left(\frac{\dot{a}}{a}\right)^2 = \frac{8}{3}\pi G\rho + \alpha_0 a^{2\beta_0 - 4}e^{\gamma^\pm(t)} \,, \tag{19}$$

where α_0 denotes an integration constant and its value is set to 1 without loss of generality. Concerning the total energy ρ, we denote $\rho = \rho_{mat} + \rho_{rad}$, which are the matter and radiation energy densities. The γ-exponent in the exponential function in Eq.(19) is defined as $\gamma^\pm(t) = \pm\sqrt{|4\eta_0 a^4 - 3|} \mp \sqrt{3}\arctan\left(\frac{\sqrt{3}}{3}\sqrt{|4\eta_0 a^4 - 3|}\right)$. The parameter β_0 inflicts on the magnitude of the deceleration parameter $q(z)$ in function of the redshift z and the parameter η_0 measures the width of the transition phase redshift z_t from a decelerating to accelerating regime. Moreover, we can write Friedman equations as

$$H(z) = H_0\sqrt{\Omega_m(z) + \Omega_{rad}(z) + \Omega_{ext}(z)} \,, \tag{20}$$

where $H(z)$ is the Hubble parameter in terms of redshift z and H_0 is the current value of the Hubble constant. The matter density parameter is denoted by $\Omega_m(z) = \Omega^0_m(1+z)^3$, $\Omega_{rad}(z) = \Omega^0_{rad}(1+z)^4$ and the term $\Omega_{ext}(z) = \Omega^0_{ext}(1+z)^{4-2\beta_0}\gamma_0$ stands for the density parameter associated with the extrinsic curvature. The upper script "0" indicates the present value of any quantity.

The transition redshift can be found from the deceleration parameter in a form

$$q(z) = \frac{1}{H(z)}\frac{dH(z)}{dz}(1+z) - 1 \,. \tag{21}$$

Hence, we can write

$$q(z) = \frac{3}{2}\left[\frac{\Omega_m(z) + \Omega_{rad}(z) + \gamma^*\Omega_{ext}(z)}{\Omega_m(z) + \Omega_{rad}(z) + \Omega_{ext}(z)}\right] - 1 \,, \tag{22}$$

where $\gamma^* = \frac{1}{3}\left[4 - 2\beta_0 \pm 2\sqrt{|\frac{4\eta_0}{(1+z)^4} - 3|}\right]$. Hence, taking Eq.(22) with the value $q = 1/2$ related to matter-dominated

Preprints (www.preprints.org) | NOT PEER-REVIEWED | Posted: 8 May 2019 doi:10.20944/preprints201905.0097.v1

era, we can obtain an estimative for the magnitude of the transition redshift z_t given by

$$z_t = |\left(\frac{4}{3}|\eta_0|\right)^{(1/4)} - 1| \, . \tag{23}$$

In this work, we investigate a late-time transition redshift $z_t \gtrsim 1$. To this end, we perform a Puiseux-Mclaurin expansion around $\eta_0 \to 0$ truncating at second order, i.e, $e^{\gamma(x(a))} \sim 1 + \frac{\sqrt{3}}{3}x(a)^{3/2} + \mathcal{O}(x^{5/2})$. After linearizing, it gives roughly $e^{\gamma(z)} \sim \gamma_0(z+1)^{-4}$, which γ_0 is a constant (with a η_0 parameter including in it). The convergence of $e^{\gamma(a)}$ is in compliance with the Walsh theorem on convergence of analytic approximations (Walsh, 1928).

The current extrinsic contribution Ω^0_{ext} is given by the normalization condition for redshift at $z = 0$ that results in

$$\Omega^0_{ext} = \gamma_0 \left(1 - \Omega^0_m - \Omega^0_{rad}\right) \, . \tag{24}$$

Hence, we can write the dimensionless Hubble parameter $E(z)$ as

$$E^2(z) = \Omega^0_m(1+z)^3 + \Omega^0_{rad}(1+z)^4 \quad + \\ \left(1 - \Omega^0_m - \Omega^0_{rad}\right)(1+z)^{-2\beta_0} \, , \tag{25}$$

3 OBSERVATIONAL CONSTRAINTS: ANALYSIS AND RESULTS

3.1 Cosmological data

The methodology used to handle the data relies on the Markov Chain Monte Carlo (MCMC) technique based on the Metropolis-Hasting algorithm. We perform our analysis using the joint likelihood of the CMB Planck 2015 data (Planck Collaboration, 2015), Pantheon SnIa (Scolnic et al., 2018), the Hubble parameter as a function of redshift ($H(z)$)(Zhang et al., 2014; Stern et al., 2010; Moresco et al., 2012; Chuang and Wang, 2013; Moresco, 2015; Delubac et al., 2015) and Baryonic Acoustic Oscillations (BAO) from points of the joint surveys 6dFGS (Beutler et al., 2011), SDDS (Anderson et al., 2014), BOSS CMASS (Xu et al. 2012), WiggleZ (Blake et al., 2012), MSG (Ross et al., 2015) and BOSS DR12 (Gil-Marín et al., 2016).

To apply our χ^2-statistics, we have a total of 1096 data points from the Pantheon set, CMB, BAO and Hubble parameter with the number of point of 1048, 3, 9 and 36, respectively. Hence, we use the background parameter vectors $\{\Omega_{m0}, 100\Omega_b h^2, h, \beta_0, \eta_1\}$, which the adopted priors were $\{(0.001, 1), (0.001, 0.08), (0.4, 1), (-1, 1), (0.2979, 0.6075)\}$, respectively. For convenience, we denote $\eta_1 = 100\eta_0$. Moreover, we adopt the following quantities implemented in the MCMC chains, like the equivalence number for the expansion factor a_{eq} given by

$$a_{eq} = \frac{1}{(1 + 2.5 * 10^4 \Omega_m h^2 (Tcmb/2.7)^{-4}} \tag{26}$$

with the sound speed c_s, redshift at decoupling z_{cmb} and drag redshift z_{drag} in a form, respectively,

where c is the speed of light. The CMB temperature we adopt the value $T_{cmb} = 2.7255K$. Moreover, the joint analysis was implemented by the product of the particular likelihoods $\mathcal{L}$ for each data set

$$\mathcal{L}_{tot} = \mathcal{L}_{Pantheon}.\mathcal{L}_{BAO}.\mathcal{L}_{CMB}.\mathcal{L}_{H(z)} \, , \tag{27}$$

and the sum of individual χ^2 to get the related total χ^2

$$\chi^2_{tot} = \chi^2_{Pantheon} + \chi^2_{BAO} + \chi^2_{CMB} + \chi^2_{H(z)}. \tag{28}$$

The adopted values for the $H(z)$ data can be found in Table 1 of the ref.(Arjona, Cardona and Nesseris, 2019). The related absolute magnitude M is given by

$$m(z) = M + 5\, log_{10}[\frac{d_L(z)}{Mpc}] + 25 \tag{29}$$

The luminosity distance D_L is defined by

$$D_L(z) = \frac{H_0 d_L(z)}{c} \tag{30}$$

as

$$m(z) = \bar{M}(M, H_0) + 5\, log_{10}(D_L(z)) \tag{31}$$

where $\bar{M}$ is the magnitude zero point offset and depends on M and H_0 as

$$\bar{M} = M + 5\, log_{10}(\frac{c/H_0}{1Mpc}) + 25 \tag{32}$$

The $\bar{M}$ is model independent and its value comes from a specific good fit that can be used directly to other fits of model parameters. Hence, the observed $m_i(z_i)$ can be translated to $D^{obs}_{Li}(z_i)$ and its value $D^{th}_L(z)$ of a given model $H(z; a_1, ..., a_n)$ can be obtained by integrating

$$D^{th}_L(z) = (1+z)\int_0^z dz' \, \frac{H_0}{H(z'; a_1, ...a_n)} \tag{33}$$

The best fit values for the parameters $a_1, ..., a_n$ are found by minimizing the quantity

$$\chi^2(a_1, ..., a_n) = \sum_{i=1}^{N} \frac{(log_{10}D^{obs}_L(z_i) - log_{10}D^{th}_L(z_i))^2}{(\sigma_{log_{10}D_L(z_i)})^2 + (\frac{\partial log_{10}D_L(z_i)}{\partial z_i}\sigma_{z_i})^2} \tag{34}$$

where σ_z is the 1σ redshift uncertainty of the data and $\sigma_{log_{10}D_L(z_i)}$ is the corresponding 1σ error of $log_{10}D^{obs}_L(z_i)$.

3.2 Results

In order to avoid an error-prone fit-to-data, we must correlate the parameters β_0 and η_0. To this matter, we define a parameterization in a form

$$\beta(a) = -1 - \frac{2}{3}\beta_0 + \eta_0(1-a). \tag{35}$$

Accordingly, the values of β_0 runs from -1 to 1 which means roughly $-1/3 \leqslant w \leqslant -1.2$, i.e, in fluid context, it is varying from quintessence to phantom fluid models. The ΛCDM model corresponds to $w = -1$ or, equivalently, $\beta_0 = 0$ in Eq.(35). We compare our results with three phenomenological models to ascertain on how the β-model is constrained to the available data. In table 1, we present the values of parameters of the ΛCDM model, and wCDM and CPL parameterisations. In figures 1 and 2, the comparisons are made with the models from a left-to-right sequence in the panels.

In figure 1, we present the obtained σ-contours with $68,3\%$, $95,4\%$ and $99,7\%$ confidence levels (C.L.) in the $(\beta_0 - \Omega_m)$ plane. In the first and third panels, we have the comparison of the model with ΛCDM and CPL with the marginalized β_0 within the 1-σ contour (light blue), and the limiting 1-σ border in the case of wCDM. The same pattern occurs in the figure 3 for the studied correlation between models, which may represent a mild tension between

Preprints (www.preprints.org) | NOT PEER-REVIEWED | Posted: 8 May 2019 doi:10.20944/preprints201905.0097.v1

Table 1. A summary of best-fit values background parameters calculated by using MCMC chains with the main parameters and resulting χ^2 values. The χ^2_{min} denotes the χ^2 best-fit value from MCMC and χ^2_{tot} refers to the value of the total χ^2 from minimizing all data. For the sake of convenience, we refer the present model in this paper as β-model as shown below. As a matter of convenience, we denote η_1 to define $\eta_0 = 100\eta_1$.

Model	Ω_{m0}	$\Omega_{b0}h^2$	h	DE parameters	χ^2_{min}	χ^2_{tot}
ΛCDM	0.3154± 0.0061	0.0222± 0.0001	0.6728± 0.0048	$w = -1$	1809.67	1809.75
wCDM	0.3163± 0.0081	0.0223± 0.0015	0.6717± 0.0074	w=-0.9927± 0.0268	1809.81	1809.75
CPL	0.3143± 0.0061	0.0223± 0.0001	0.6751± 0.0004	w=-0.9998± 0.0008 wa=-0.0166± 0.0080	1809.69	1809.75
β-model	0.3133± 0.0069	0.0222± 0.0002	0.6750± 0.0062	β_0=-0.0099± 0.0341 η_1=0.3044± 0.0042	1809.58	1809.80

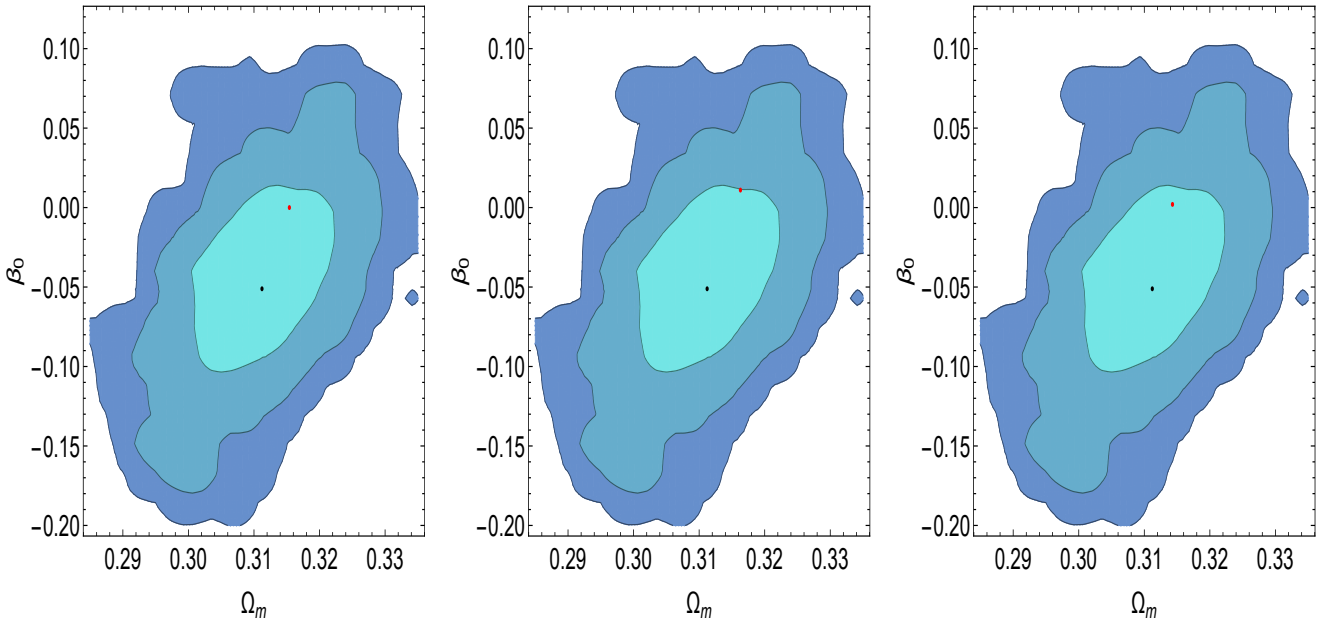

Figure 1. Contour regions at 1-σ, 2-σ and 3-σ at 68, 3%, 95, 4% and 99, 7% C.L. in the $(\beta_0 - \Omega_m)$ plane. The points represents the mean values of the parameters in the MCMC chain. The red dots denote the β-model and the black dots denote the comparison models and from left-to-right, we have ΛCDM, wCDM and CPL models, respectively.

Table 2. A summary of mean values of background parameters calculated by using MCMC chains with the main parameters.

Model	Ω_{m0}	$\Omega_{b0}h^2$	h	DE parameters
ΛCDM	0.3179± 0.0065	0.0223± 0.0001	0.6694± 0.0051	$w = -1$
wCDM	0.3163± 0.0081	0.0223± 0.0015	0.6717± 0.0074	w=-0.9927± 0.0268
CPL	0.3134± 0.0062	0.0222± 0.0001	0.6752± 0.0046	w=-0.9996± 0.0008 wa=-0.0166± 0.008
β-model	0.3158± 0.0097	0.0222± 0.0003	0.6730± 0.0082	β_0=-0.0133± 0.0876 η_1=0.3083± 0.0051

Table 3. A summary of the obtained values of AIC and BIC for the studied models.

Model	AIC	ΔAIC	Tension	BIC	ΔBIC	Tension
ΛCDM	1817.71	1.93	weak	1837.67	6.91	growing
wCDM	1817.85	1.79	weak	1837.81	6.77	growing
CPL	1819.75	0.11	mild	1844.69	0.11	mild
β-model	1819.64	0	-	1844.58	0	-

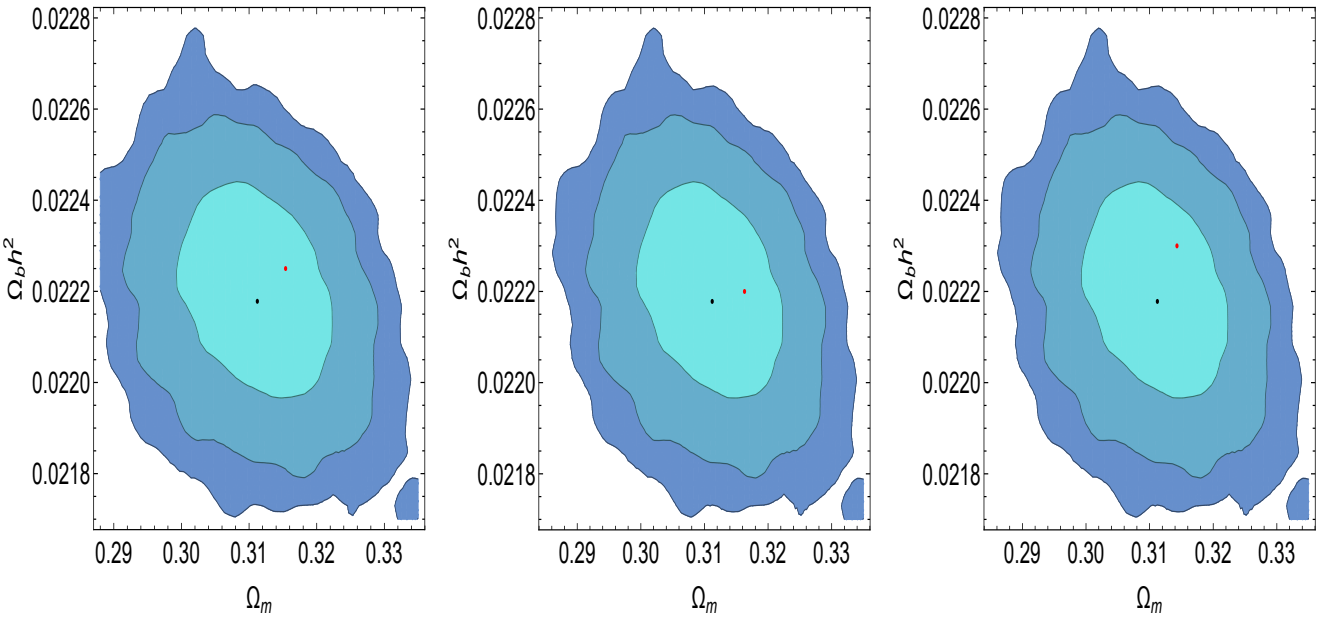

Figure 2. Contour regions at 1-σ, 2-σ and 3-σ at $68,3\%$, $95,4\%$ and $99,7\%$ C.L. in the $(\Omega_b h^2 - \Omega_m)$ plane.

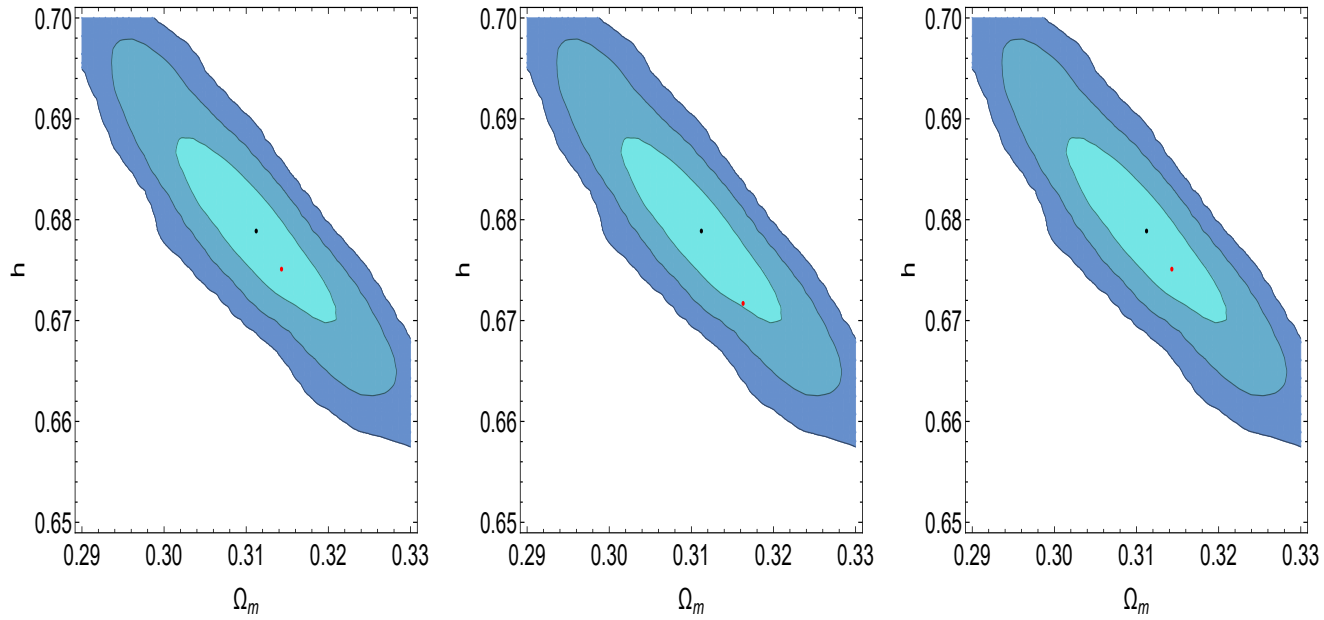

Figure 3. Contour regions at 1-σ, 2-σ and 3-σ at $68,3\%$, $95,4\%$ and $99,7\%$ C.L. in the $(h - \Omega_m)$ plane. The points represents the mean values of the parameters in the MCMC chain.

low redshift data ($H(z)$) and the Planck probe (Nesseris, Pantazis and Perivolaropoulos 2017; Arjona, Cardona and Nesseris, 2019). In the figure 2, a comparison with the accommodation of the baryonic luminous matter parameter $\Omega_b h^2$ with the distribution of the matter density parameter Ω_m, we have a well-behaved predictions at 1-σ level for all models in the plane $(\Omega_b h^2 - \Omega_m)$.

In order to classify the correlation between models, we adopt the errors being as Gaussian. Thus, we use AIC systematic to classify the fit-to-data for small samples sizes (Sugiura, 1978; Liddle, 2007)

$$AIC = \chi^2_{bf} + 2k\frac{2k(k+1)}{N-k-1}\,, \tag{36}$$

where χ^2_{bf} is the best fit χ^2 of the model, k represents the number of the free parameters and N is the number of the data point in the adopted dataset. The difference $|\Delta AIC| = AIC_{model\ 2} - AIC_{model\ 1}$ obeys the Jeffreys' scale (Jeffreys, 1961) that measures the intensity of tension between two competing models. In general, higher values for $|\Delta AIC|$ denotes more tension between models, that means a higher statistical distance and the models are not statistically compatible.

Preprints (www.preprints.org) | NOT PEER-REVIEWED | Posted: 8 May 2019 doi:10.20944/preprints201905.0097.v1

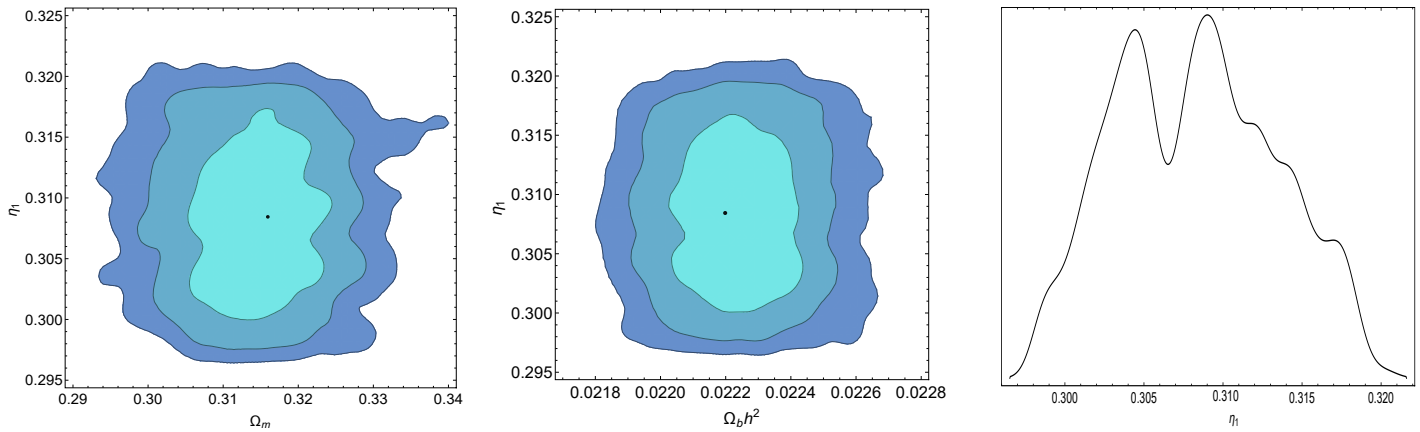

Figure 4. Contour regions at 1-σ, 2-σ and 3-σ at $68,3\%$, $95,4\%$ and $99,7\%$ C.L. in the $(\eta_1 - \Omega_m)$ and $(\eta_1 - \Omega_b h^2)$ planes. The black points represent the mean values of the η_1 parameter in the MCMC chain. The third figure (right panel) represents the 1-d probability of distribution function of η_1 parameter.

In summary, the Jeffreys' scale can be set in the following: for $|\Delta AIC \leqslant 2|$ the models are statistically consistent and equivalents. For $4 < \Delta AIC < 7$ and $|\Delta AIC \geqslant 10|$ induces to growing tension between the models with positive evidence and strong evidence against the equivalence of the models, respectively. Accordingly, we have obtained the values for the β-ΛCDM with 1.93, and β-wCDM and β-CPL with AIC 1.79 and 0.11, respectively. This result leads to the conclusion that the β-model favors CPL parameterization with a lower AIC, even though it is shown that the β-model is statistically consistent (weak tension) with ΛCDM and wCDM models. Likewise, we apply BIC classifiers (Schwarz, 1978) that work well for independent homogeneous distribution of datasets (Liddle, 2007). Unlike AIC, the BIC method heavily penalizes free parameters of a model. Thus, we use the following formula

$$BIC = \chi^2_{bf} + k \ln N \,, \tag{37}$$

where χ^2_{bf} is the best fit χ^2 of the model, k represents the number of the free parameters and N is the number of the data point in the adopted dataset. Therefore, from Jeffrey's scale, a smaller BIC values favor statistically better models (lower tension between two comparison models). In these terms, we have similar results as those obtained from AIC, with ΔBIC of the order of 0.11, except for the cases of ΛCDM and wCDM which the comparison in BIC analysis gives the values 6.91 and 6.77 indicating a growing tension between the models. Particulary, the tension is a little higher with the ΛCDM model, that shows a non-preferable tendency for non-dynamical dark energy models, besides the fact that the BIC analysis has a severe sensitivity on free parameters. The table III shows a summary of AIC and BIC values for the models and the corresponding tension between the models.

In the figure 04, we present the marginalized η_0 in the $(\eta_1 - \Omega_m)$ and $(\eta_1 - \Omega_b h^2)$ planes, where, $\eta_0 = 100\eta_1$ that reflects are good concordance with recent estimates for the matter density parameter. The obtained best-fit $\eta_1 = 0.3083 \pm 0.0051$ values define the transition redshift range $z_t = 1.5321 \pm 0.17$. In the third panel, it shows a likelihood with several minima and the preferred one consists in the second minima that it is in accordance with the former parameters. This behaviour of η_0, which is related to z_t may be related with the appearances of numerical degeneracies with data (BAO, for example, is sensitive to intermediate redshifts) besides the fact that the transition redshift naturally presents degeneracies. For a larger z_t, the likelihood decays into a long tale, but for smaller z_t, it may indicate changes in the integrated Sachs-Wolfe (ISW) contribution, leading to a different signature of the star-formation in detriment of ΛCDM prediction, which will be investigated further.

4 REMARKS

In this paper, we discussed the dark energy problem with a proposal of a geometric model for the accelerated expansion. By construction, we used the Nash-Green theorem to propose a geometric model with a resulting modified Friedman equation from the influence of the extrinsic curvature thought as a complement to Einstein's gravity. Starting from the possibility to relate one free parameter to the redshift transition z_t, we investigated the possibility that the equation of state undergoes to intermediate redshifts $1 \lesssim z_t \lesssim 2$ eventually. In all cases, we applied the AIC and BIC classifies and we found that the model favours the CPL parameterization. Interestingly, we obtained that the transition redshift acts like a good tuning parameter in the acceleration expansion and may be used as a cosmic descriptor. This transition occurred in intermediate redshift $z_t = 1.5321 \pm 0.17$ with a marginalized $\eta_0 = 100\eta_1$ for the best-fit $\eta_1 = 0.3083 \pm 0.0051$ at 1-σ C.L.. This value defines that the transition redshift range may inflict changes in the ISW contribution as different as the one as predicted to ΛCDM with a lower peak of the second CMB peak. As future prospects, we intend to investigate the evolution of the background with the evaluation of the evolution equations of the perturbations in conformal Newtonian gauge confront the behaviour of the viscosity parameter and growth index rate resulting from the model for a realistic one. This process is in due course and will be reported elsewhere.

5 ACKNOWLEDGMENTS

The author thanks Federal University of Latin-American Integration for financial support from Edital PRPPG 110 (17/09/2018) and Fundação Araucária/PR for the Grant CP15/2017-P&D 67/2019.

REFERENCES

Ade P. A. R. et al., (Planck Collaboration), 2016, Astron. Astrophys. 594, A13.
Akaike H., 1974, IEEE Transactions of Automatic Control, 19, 716.
Anderson L. et al., 2014, (BOSS collaboration), Mon. Not. Roy. Astron. Soc.441, 24.
Arkani-Hamed N., Dimopoulos S., Dvali G., 1998, Phys. Lett., B429, 263.
Arjona R., Cardona W., Nesseris S., 2019, Phys. Rev. D 99, 043516.
Battye R. A., Carter B., 2001, Phys. Lett. B, 509, 331.
Bassett A. B., Kunz M., Silk J., Ungarelli C., 2002, Mon. Not. R. Astron. Soc. 336, 1217-1222.
Blake C. et al., 2012, Mon. Not. Roy. Astron. Soc. 425, 405.
Beutler F. et al., 2011, Mon. Not. Roy. Astron. Soc. 416, 3017.
Caldwell R. R., Dave R., Steinhardt P. J., 2018, Phys. Rev. Lett. 80, 1582.
Capistrano A. J. S., Cabral L. A., 2014, Ann. Phys., 384, 64-83.
Capistrano A. J. S., 2015, Montl. Not. Roy. Soc, 448, 1232-1239.
Capistrano A. J. S., Cabral L. A., 2016, Class. Quantum Grav. 33, 245006.
Capistrano A. J. S., Gutiérrez-Pieres A. C., Ulhoa S. C., Amorim R. G. G., 2017, Ann. Phys., 380, 106120.
Capistrano A. J. S., Ann. Phys. (Berlin), 1700232, (2017).
Chevallier M., Polarski D., 2001, Int. J. Mod. Phys. D 10, 213.
Chuang C.H., Wang Y., 2013, Mon. Not. Roy. Astron. Soc. 435, 255.
Delubac T. et al. (BOSS collaboration), 2015, Astron. Astrophys. 574, A59.
Di Valentino E., Linder E. V., Melchiorri A., 2018, Phys. Rev. D97, 043528.
Donaldson S. K., 1984, Contemporary Mathematics (AMS), 35, 201.
Durrive J.-B., Ooba J., Ichiki K., Sugiyama N., 2018, Phys. Rev. D97, 043503.
Dvali G., Gabadadze G., Porrati M., 2000, Phys. Lett.B485, 208-214.
Gil-Marín H. et al., 2016, Mon. Not. Roy. Astron. Soc. 460, 4210.
Greene R., 1970, Memoirs Amer. Math. Soc., 97.
Gupta S. N., 1954, Phys. Rev., 96, 6.
Heydari-Fard M., Sepangi H. R., 2007, Phys.Lett.B649, 1-11.
Hill C.T., Schramm D. N., Fry J.N., 1988, Comments Nucl. Part. Phys., 19, 25, 407.
Holdom B., 1983, *the cosmological constant and the embedded universe*, Standford preprint ITP-744.
Jeffreys H., 1961, Theory of Probability, 3rd edn. Oxford Univ. Press, Oxford.
Kumar P., Singh C. P., 2017, Astrophys Space Sci., 362, 52.
Jalalzadeh S., Vakili B., Sepangi H. R., 2007, Phys. Scr., 76, 122.
Jalalzadeh S., Mehrnia M., Sepangi H. R., 2009, Class.Quant.Grav., 26,155007.
Liddle A. R., 2007, Mon. Not. R. Astron. Soc. 377, L74L78.
Lim C. S., 2014, Prog. Theor. Exp. Phys., 02A101.
Linder E. V., 2003, Phys. Rev. Lett., 90, 091301.
Nesseris S., Pantazis G., Perivolaropoulos L., 2017, Phys. Rev. D 96, 023542.
Luna C. A., Basilakos S., Nesseris S., 2018, Phys. Rev. D 98, 023516.
Maia M. D., Monte E. M., 2002, Phys. Lett. A, 297, 2, 9-19.
Maia M.D., Monte E.M., Maia J.M.F., Alcaniz J.S., 2005, Class.Quantum Grav., 22, 1623.
Maia M.D., Silva N., Fernandes M.C.B., 2007, JHEP, 04, 047.
Maia M. D., Capistrano A. J. S., Alcaniz J. S., Monte E. M., 2011, Gen. Rel. Grav., 10, 2685.
Maia M. D., 2011, *Geometry of the fundamental interactions*, Springer: New York, p.166.
Mortonson M. J., Hu W., Huterer D., 2009, Phys. Rev. D80, 067301.
Martins C. J. A. P., Colomer P. M., 2016, A&A, 594, A14.
Martins C. J. A. P., Colomer P. M., 2018, A&A, 616, A32.
Martins C. J. A. P., Colomer P. M., 2019, Phys. Lett. B, 791, 230-235.
Moresco M. et al., 2012, JCAP 1208, 006.
Moresco M., 2015, Mon. Not. Roy. Astron. Soc. 450, L16.
Nash J., 1956, Ann. Maths., 63, 20.
Nemiroff R. J., Joshi R., Atla B.R., 2015, JCAP06, 006.
Nozari K., Behrouz N., Rashidi N., 2014, Adv. High En.Phys., Article ID 569702.
Parker L., Raval A., 1999, Phys. Rev. D60, 123502, 1999 [Erratum: Phys. Rev.D67,029902 (2003).
Parker L., Raval A., 2000, Phys. Rev. D62, 083503. [Erratum: Phys. Rev.D67,029903(2003)]
Randall L., Sundrum R., 1999, Phys. Rev. Lett. 83, 3370.
Randall L., Sundrum R., 1999, Phys. Rev. Lett., 83, 4690.
Ranjbar A., Sepangi H. R., Shahidi S., 2012, Ann. Phys., 327, 3170-3181.
Ratra B., Peebles P. J. E., 1988, Phys. Rev. D 37, 3406.
Ross A. J. at al., 2015, Mon. Not. Roy. Astron.Soc. 449, 835.
Santos B., Coley A. A., Devi C. N., Alcaniz J.S., 2017, JCAP02, 047.
Schwarz G., 1978, Ann. Statist., 5, 461.
Scolnic D. M. et al., 2018, Astrophys. J. 859, 101 (2018), 1710.00845.
Sivanandam N., 2013, Phys. Rev. D 87, 083514.
Stern D., Jimenez R., Verde L., Kamionkowski M., Stanford S. A., 2010, JCAP 1002, 008.
Sugiura N., 1978, Communications in Statistics A, Theory and Methods, 7, 13.
Sultana J., 2016, Mon.Not.Roy.Astron.Soc. 457(1), 212-216.
Taubes C. H., 1984, Contemporary Mathematics (AMS), 35, 493.
Turner M. S., White M., 1987, Phys. Rev. D56, 4439.
Walsh J. L., 1928, Trans. Amer. Math. Sot. 30, 307-332.

Velten H.E.S., vom Marttens R.F., Zimdahl W., 2014, Eur.Phys.J. C74, 11, 3160.
Xu X., Padmanabhan N., Eisenstein D. J., Mehta K. T., Cuesta A. J., 2012, Mon. Not. Roy. Astron. Soc. 427, 2146.
Zhang C., Zhang H., Yuan S., Zhang T. J., Sun Y.-C., 2014, Res. Astron. Astrophys. 14, 1221, 1207.4541.